PAPER

Profiling of Modified Chitosan-Based Composites as Tetracycline Hydrochloride Drug Release Systems

Nurul Anjartikasari[1], Emmy Yuanita[1], Ni Komang Tri Dharmayani[1], Sudirman[1], Ni Made Sudewianingsih[2], and Maria Ulfa[1*]

Abstract. Controlled drug release systems (DRS) are a crucial technology in the medical field, and they continue to be developed today. Chitosan is useful in manufacturing-controlled drug release systems due to its non-toxic, biodegradable, and biocompatible properties. However, it has some limitations when it comes to its physical and mechanical properties. Combining chitosan with other materials, such as bacterial cellulose (BC), graphite (Gr), ZnO, and TiO_2, can improve its mechanical properties and antibacterial activity. This study aims to synthesize $Chi/BC/Gr/TiO_2$ and $Chi/BC/Gr/ZnO$ composites as drug release systems. When tested with TCH, an antibiotic model, the drug release kinetics of the composite followed the Hixson-Crowell and Korsmeyer-Peppas kinetics models. Additional tests for physical and mechanical properties, as well as antibacterial activity, have also been conducted. Mechanical properties in terms of tensile strength and Young's modulus in composites with adding Gr, TiO_2, and ZnO have higher values than Chi/BC alone. Compared to positive control, both TCH-loaded composites show higher inhibition against *S. aureus* bacteria. Based on the results of this study, composite $Chi/BC/Gr/TiO_2$ and $Chi/BC/Gr/ZnO$ have potential applications as DRS such as wound dressing.

Introduction

Controlled drug release systems are a technology currently being developed for use in the medical field. These systems are designed to release drugs within a specific period, providing long-term therapeutic effects (Adepu & Ramakrishna, 2021). These systems aim to maintain a steady drug concentration within the minimum effective and maximum safe concentrations in a certain period, resulting in optimal drug performance (Laracuente et al., 2020). To create controlled drug release systems, various polymeric materials such as nanoparticles and hydrogels are used in their manufacture (Rahimi et al., 2021).

Chitosan (Chi) is a type of polysaccharide amino organic material. It is a polymer that can be used as a controlled drug-release system (Lu et al., 2022). Biocompatibility, biodegradability and non-toxicity are the unique properties of chitosan (Fakhri et al., 2020), which makes it suitable for medical applications. It also exhibits antibacterial activity against gram-positive and gram-negative bacteria (Li et al., 2020). However, its poor mechanical properties have limited its potential for use in the medical field. To overcome this issue, a combination of crosslinking agents, plasticizing agents, and other polymers can be used, or chitosan can be made into composites (Wahba, 2020). One of the materials that can be used as a reinforcing agent in composite manufacturing is Bacterial cellulose (BC) (Choi & Shin, 2020). It has excellent mechanical properties, high biodegradability, biocompatibility, and high purity. Combined with Chi, it produces composites with much stronger mechanical properties than pure chitosan (Wahid et al., 2019).

The addition of specific inorganic materials such as graphite (Gr), TiO_2, and ZnO can significantly enhance the mechanical properties of Chi. Studies have demonstrated

[1]Departement, Faculty of Mathematics and Natural Science, University of Mataram, Mataram-NTB, 83125 Indonesia; **Email: ulfaarief@unram.ac.id**
[2]Biology Laboratory, Faculty of Mathematics and Natural Science, University of Mataram, Mataram-NTB, 83125 Indonesia

that adding graphitic materials, such as graphene oxide, can increase the tensile strength and Young's modulus of chitosan (Tavakoli et al., 2020). Additionally, graphitic materials have been found to improve the drug-loading capability of composites because it has hydrophobic properties and can load the drug by noncovalent adsorption through π-π stacking interaction (Hosseini et al., 2022). Similarly, introducing TiO_2 can enhance the antibacterial activity and tensile strength of Chi (Hussein et al., 2021). The same improvement can be seen in Chi by adding ZnO (Kalemtas et al., 2022).

Chitosan-based composites have been developed to carry antimicrobial agents (Fasiku et al., 2021), including antibiotics, like tetracycline hydrochloride (TCH) (El-Alfy et al., 2020). A recent study found that the chitosan-based composite can adsorb TCH (Turan et al., 2022). TCH is a broad-spectrum antibiotic used to treat bacterial infections such as periodontitis, bone infections, and skin treatment (Farzamfar et al., 2019; Mirzaeei et al., 2022; Orylska-Ratynska et al., 2022). However, it is hydrophilic and water-soluble, so its release from the composite must be controlled for continuous treatment. This controlled release is also essential to prevent exceeding the maximum safe concentration that can cause cytotoxicity. Additionally, controlled release can reduce the potential for resistance to the antibiotic, thus preventing a decrease in its effectiveness ((Chahardahmasoumi et al., 2019).

This research aims to create controlled drug release systems by producing chitosan-based composites: $Chi/BC/Gr/TiO_2$ and Chi/BC/Gr/ZnO. The drug release kinetics of these composites were analyzed to determine each system's kinetics model and drug release mechanism. Tetracycline HCl was employed as the model antibiotic to examine the drug release kinetics. Additionally, the antibacterial activity, physical properties, and mechanical properties of the composites were also evaluated in this study.

Experimental

Material and Methods

The materials used for this study included chitosan, bacterial cellulose (obtained from UMKM NATA Yogyakarta Farahshop, Yogyakarta), glacial acetic acid (Merck), maltodextrin, graphite, TiO_2 (Merck), ZnO (Merck), TCH drug (PT. Novapharin Pharmaceutical Industries), 96% ethanol, NaOH, n-butanol, and pH buffer solutions with values of 1.2, 4.5, 6.86, 7.4, and 8.4.

The research was conducted using a standard set of glassware and equipment. This includes a hot plate stirrer (IKA C-MAG HS 7), ultrasonication device (Trias Anatomy Chemindo), oven (Memmert), furnace (Thermoscientific),

blender (Miyako), analytical balance (Fujitsu FSR-A220), porcelain crucible, spatula, digital screw micrometer (T&E CR1632), and pH meter (RoHS). In addition, instrumentation tools such as FTIR spectroscopy (Perkin Elmer), UV-Vis (Thermofisher), EDS (JEOL JCM-7000), and tensilon (Instron 5567) were used for the research.

Procedures

Synthesis of Composites

The process of synthesizing chitosan-based composites followed the method of Wahid et al. (2019) with some modifications. A solution of 2.78% (b/v) chitosan in 1% (v/v) glacial acetic acid was stirred using a stirrer for 30 minutes. BC slurry 5% (b/v) and maltodextrin solution 10% (b/v) were added to the chitosan solution as cross-linking agents. Calcined graphite powder (1000 °C, 5 min) with a concentration of 0.5% (w/v) was gradually added to the Chi/BC mixture and stirred rapidly for 30 minutes, resulting in a Chi/BC/Gr mixture. To obtain $Chi/BC/Gr/TiO_2$ and Chi/BC/Gr/ZnO composites, TiO_2 and ZnO were added using the method of Rais et al. (2022) with modifications. TiO_2 powder 1% (w/v) and ZnO 1% (w/v) were each dispersed into 96% (v/v) ethanol. The resulting dispersion was added to the Chi/BC/Gr mixture while stirring for 30 minutes. The mixture was molded in a petri dish and oven-dried at 40°C.

Physical and Mechanical Test of Composites

The composite material underwent physical and mechanical testing. Physical testing included thickness, porosity, and swelling tests, while automated testing included tensile strength and Young's modulus tests. The thickness test was conducted by measuring the composite's thickness at ten different points using a digital screw micrometer. The results were then averaged using Equation 1, where $\bar{t}$ represents the average thickness and t represents the thickness value of each measurement. Mechanical tests were performed with a tensilon. This testing was carried out using the methodology of Cai et al. (2020).

$$\bar{t} = \frac{(t_1 + t_2 + ... + t_{10})}{10} \quad (1)$$

The porosity measurement was carried out using the immersion method in n-butanol. The porosity value of the composite was calculated by equation 2, where φ is the porosity percentage, m_2 is the mass of the composite after immersion, m_1 is the mass before immersion, ρB is the density of butanol, and V_k is the volume of the composite (Xu et al., 2019).

$$\phi = \frac{(m_2 - m_1)/\rho_B}{((m_2 - m_1)/\rho_B) + V_K} \qquad (2)$$

The material is soaked in a buffer solution with a specific pH level to initiate swelling. This process is carried out for a while maintaining a constant pH. Equation 3 calculates the swelling value, where m_1 is the mass of the material before soaking, and m_2 is the mass after soaking (Arikibe et al., 2021).

$$S = \frac{(m_2 - m_1)}{m_1} \times 100 \% \qquad (3)$$

EDS Analysis

EDS analysis determined each composite's atomic composition and surface structure.

FTIR Analysis

FTIR characterized the dried composites to determine each composite's specific functional groups and structure (Yasmeen et al., 2016). FTIR testing was also performed on Chi/BC and Chi/BC/Gr composites for comparison.

Drug Loading and Drug Release Kinetic Study

The drug-loading process was carried out using the adsorption method. This process follows the technique of Arikibe et al. (2021) with modifications. The drug solution was prepared by dissolving TCH in distilled water. The composite was cut (2 × 2 cm) and immersed in TCH solution (50 ppm, 24 h). The results of soaking were oven-dried (40°C). Drug release kinetics were performed by immersing the TCH-supplemented composite in pH 6.8 buffer solution for 2 hours. The concentration of TCH released from the composite was monitored every 30 minutes with a UV-Vis spectrophotometer. The absorbance of TCH was measured at a wavelength of 294 nm.

The test results of drug release by the composite were plotted by following several kinetics models. Equations 4, 5, 6, 7, and 8 show the order 0, order 1, Higuchi, Hixson-Crowell, and Korsmeyer-Peppas kinetics models used in this study, respectively. The value of Q in the equation is the concentration of the drug released, k is the drug release rate constant, t is the drug release time, M_t/M_∞ is the fractional release of the drug, and n is the diffusion exponent (Flores & Kong, 2017; Iftime et al., 2020).

$$Q = kt, \qquad (4)$$

$$\text{Log } Q = kt/2.303 \qquad (5)$$

$$Q = kt^{1/2} \qquad (6)$$

$$\left(1 - \frac{M_t}{M_\infty}\right)^{1/3} = -kt \qquad (7)$$

$$\frac{M_t}{M_\infty} = kt^n \qquad (8)$$

Result and Discussion

UV-Vis Characterization

Each composite's thickness and porosity values vary and are presented in Table 1. Different thicknesses of resulting composites can be caused by the casting or composite molding process. Composites that had TiO_2 added to them tended to be more porous than those that had ZnO added to them. The reason for this is because TiO_2 and Chi create hydrogen bonds, which increase the porosity of the composite (Fan et al., 2016). Hydrogen bonding in composite materials generally results in porous structures, which raise porosity (Laksmono et al., 2017).

Table 1. Thickness and porosity of composites.

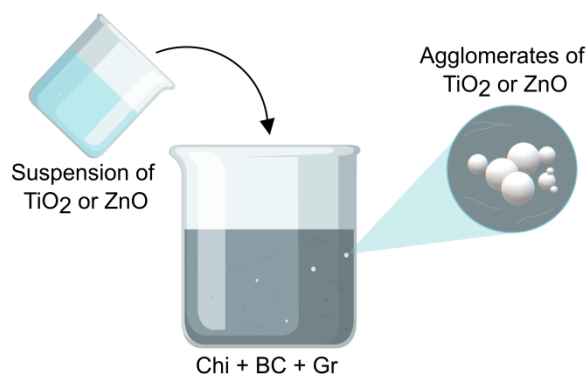| Composite	Thickness (cm)	Porosity (%)
Chi/BC/Gr/TiO_2	0.0172 ± 0.0003	19.2939 ± 5.5129
Chi/BC/Gr/ZnO	0.0212 ± 0.0036	16.1996 ± 1.3394

Figure 1. Agglomeration in The Composite's Synthesis Process.

In this study, ZnO and Chi form hydrogen bonds. On the other hand, because ZnO aggregates in the composite with a greater number of agglomerates than in Chi/BC/Gr/TiO_2, the porosity of the ZnO composite is lower than in the TiO_2 composite. Agglomerates of ZnO particles have been demonstrated in earlier studies to be able to decrease the porosity of the composite (Kamaludin et al., 2022). Figure 1 shows how the addition of TiO_2 or ZnO during the composite synthesis process causes agglomerates to develop.

The composite porosity of Chi/BC/Gr/TiO₂ and Chi/BC/Gr/ZnO is lower than the composite Chi/Cellulose from the research of Pomari et al. (2019). Table 2 shows the porosity of the Chi/Cellulose composite with 6% cellulose concentration. The lower porosity value of the composites in this study is due to the addition of Gr, TiO₂, and ZnO fillers, which reduce the pore volume in the composites. The difference in the type of crosslinker used in the previous study also affects the porosity.

Table 2. Comparison of Composites Porosity with Previous Research.

Composite	Porosity (%)
Chi/BC/Gr/TiO₂	19.29
Chi/BC/Gr/ZnO	16.20
Chi/Cellulose (Pomari et al., 2019)	51.00

Composite Swelling

Figure 2 displays the results of the swelling percentage measurement against pH changes, and Figure 3 displays the swelling results against time changes. Every composite has a maximum swelling point at a particular ideal pH level, according to the tests shown in Figure 2. At pH 7.4 and 1.2, respectively, the Chi/BC/Gr/TiO₂ and Chi/BC/Gr/ZnO composites show the highest percentage of swelling. Because ZnO has an electrical charge that generates osmotic pressure, Chi/BC/Gr/ZnO composites typically have a larger swelling percentage than Chi/BC/Gr/TiO₂ composites at all pH values. According to George et al. (2019), this pressure leads to water molecules entering the composite to make up for it. Because ZnO prefers to disintegrate in acidic environments, the maximal swelling of Chi/BC/Gr/ZnO occurs at pH 1.2.
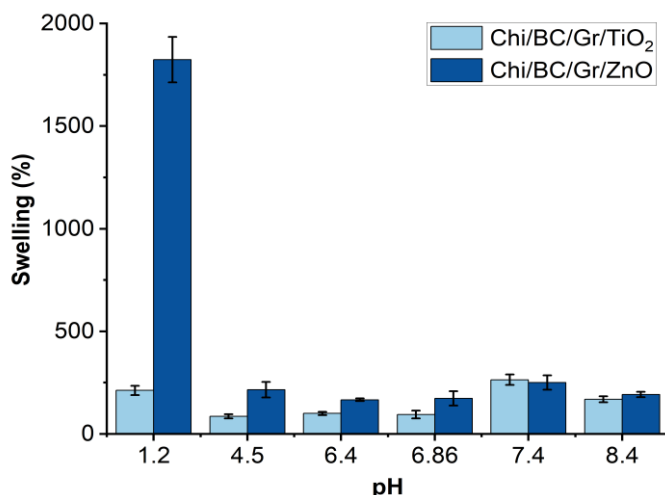

Figure 2. Swelling Percentage of Composites Against pH Changes.

A comparison study was conducted on the swelling behavior of Chi/BC composite with and without adding Gr, TiO₂, and ZnO fillers. The findings revealed that the composites with fillers were more resistant to long-term immersion in acidic (pH 1.2) and alkaline (pH 8.4) conditions than the Chi/BC composite. The Chi/BC composite degraded after 120 minutes of immersion in acidic and alkaline conditions. Adding Gr in the composites prevented matrix degradation due to its hydrophobic nature. Hydrolysis reactions can break the glycosidic bonds in Chi and BC, leading to composite degradation. However, the hydrophobic nature of Gr inhibits the hydrolysis reaction during immersion, thus preventing matrix degradation.
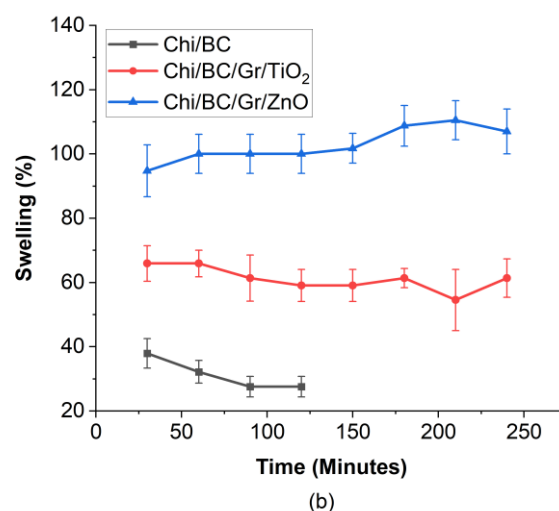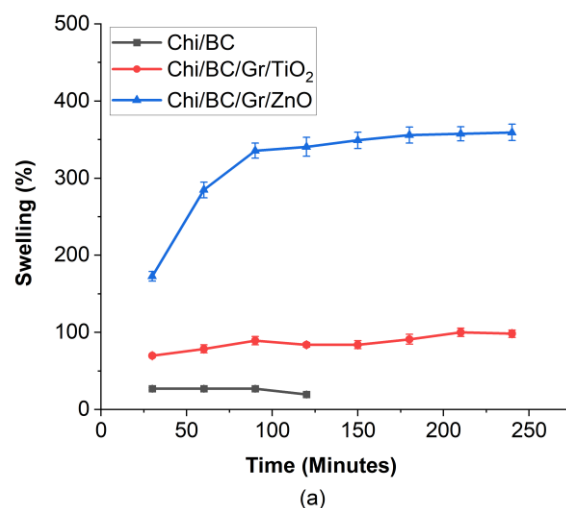

Figure 3. Swelling of Composites with Time Change in (a) Acidic and (b) Basic Conditions.

Mechanical Properties

The results of mechanical property tests, including tensile strength and Young's modulus, are presented in

Figure 4. Additionally, Chi/BC composites were tested for comparison purposes. Adding filler to composites has been found to increase their tensile strength and Young's modulus values. Specifically, adding Gr has been found to produce better mechanical properties, including higher tensile strength and Young's modulus values, compared to Chi/BC composites. This is likely due to the interfacial adhesion of Gr to Chi. Adding metal oxides can also improve the composite's mechanical properties.

The improvement in mechanical properties with the addition of TiO_2 and ZnO could be due to hydrogen bonds formed between the metal oxides and the chitosan or BC polymers, as described by Anaya-Esparza et al. (2020) and Ekanayake & Godakumbura (2021). Composites with the addition of ZnO have been found to have much higher tensile strength and Young's modulus values than those with the addition of TiO_2. This is consistent with previous research and suggests that Chi/BC/Gr/ZnO composites are harder and more pressure-resistant than Chi/BC/Gr/TiO_2 composites. These findings were reported by Yenier et al. (2016) and Suryanegara et al. (2021). The higher value of mechanical properties in the composites with ZnO addition could be due to the stronger electrostatic interaction between the $-NH_2$ group of chitosan and the Zn^{2+} ions of dissolved ZnO, compared to the electrostatic interaction between the $-NH_2$ group and Ti atoms of TiO_2.
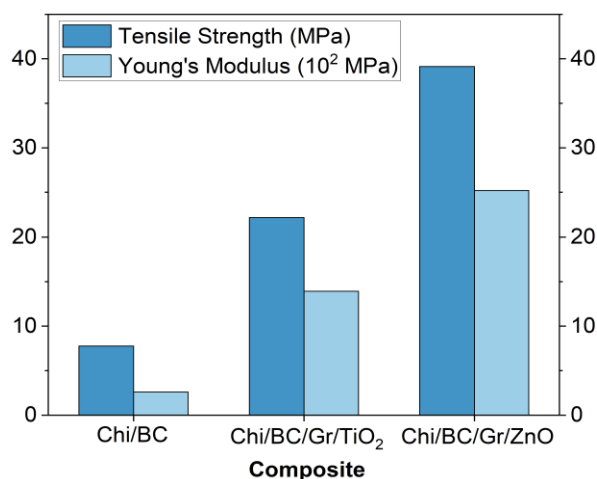

Figure 4. Tensile Strength and Young's Modulus Graphs of Composites.

Table 3 compares the tensile strength values of Chi/BC/Gr/TiO_2 and Chi/BC/Gr/ZnO with composites from a previous study. The composite Chi/BC/Gr/TiO_2 has a lower tensile strength than Chi/Cellulose/TiO_2, while the opposite is true for Chi/BC/Gr/ZnO, which has a higher tensile strength than Chi/Cellulose/ZnO. This difference could be due to the addition of Gr and the use of different methods.

Table 3. Comparison of Composites' Tensile Strength with Previous Research.

Composite	Tensile Strength (Mpa)
Chi/BC/Gr/TiO_2	22.18
Chi/Cellulose/TiO_2 (Rahmi et al., 2021)	158.57
Chi/BC/Gr/ZnO	39.14
Chi/Cellulose/ZnO (Sun et al., 2022)	10.69

EDS Analysis

The graph in Figure 5 shows that the Ti and Zn intensity peaks appear together, indicating that TiO_2 and ZnO are successfully dispersed in the composite. The graph shows that the composition of Zn atoms is almost twice as high as that of Ti atoms. This may be due to the agglomeration of ZnO at a certain point, as shown in Figure 6. This also affects the porosity of Chi/BC/Gr/ZnO, as shown in the illustration in Figure 6.
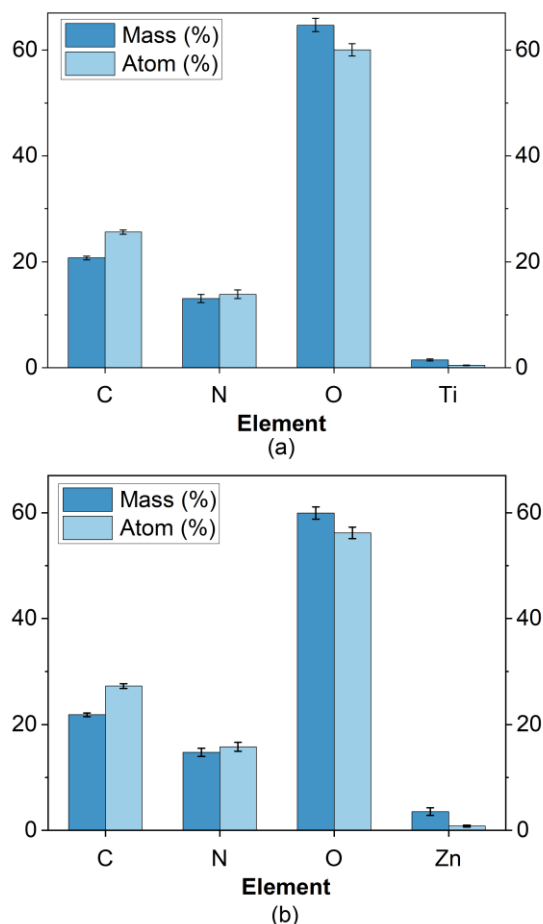

Figure 5. EDS Graph of (a) Chi/BC/Gr/TiO_2 and (b) Chi/BC/Gr/ZnO.
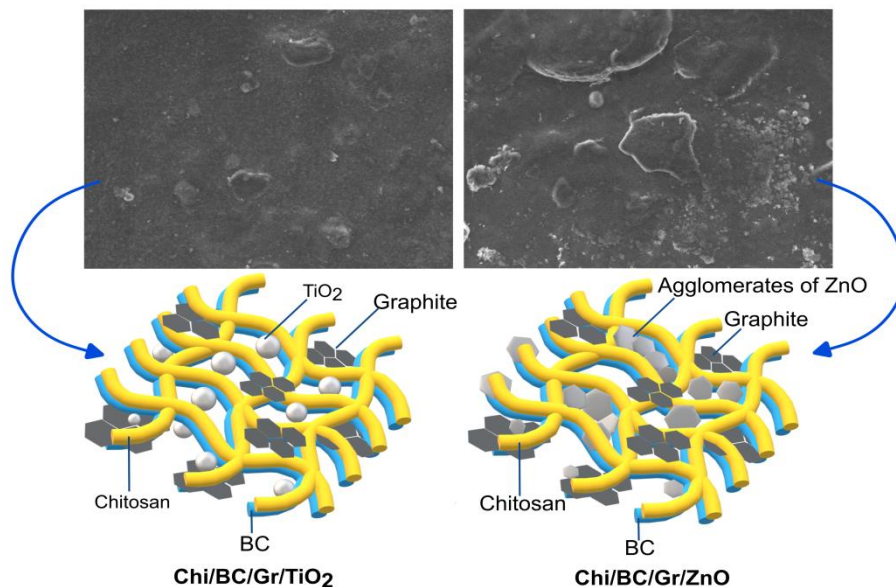
Figure 6. Chi/BC/Gr/TiO₂ and Chi/BC/Gr/ZnO Surfaces and Illustration of Composite.

Based on the information in Figure 6, the Chi/BC/Gr/TiO₂ composite surface appears flatter than that of Chi/BC/Gr/ZnO. The TiO₂ metal is also more evenly dispersed than ZnO. In the Chi/BC/Gr/ZnO composite case, the ZnO metal is clustered at one point. Additionally, Figure 6 illustrates the layers of each composite. The illustration shows that the ZnO agglomerates cover the pores of the composite, leading to a lower porosity value of Chi/BC/Gr/ZnO

FTIR Analysis

According to Figure 7, Chi/BC/Gr/TiO₂ and Chi/BC/Gr/ZnO composites had changes in the intensity and wavelength shifts of their absorption peaks compared to Chi/BC and Chi/BC/Gr composites. The FTIR spectrum of the composite showed an O-H absorption peak, which is typical for BC produced with tofu waste media (Ulfa et al., 2023). The absorption peak also came from the O-H and N-H vibrations of Chi (Wahid et al., 2019).
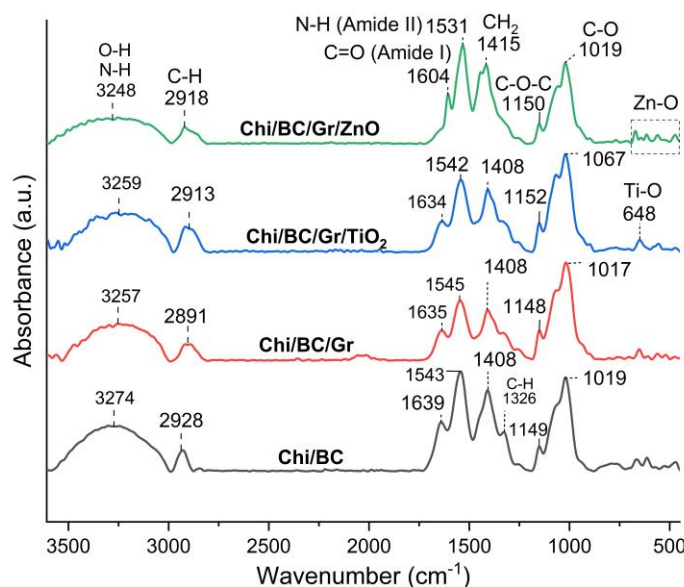

Figure 7. FTIR Spectra of Composites

Other typical absorptions of Chi include N-H stretching, N-H bending, and C-O and C-O-C vibrations of the glycoside bond and glucose ring (Anaya-Esparza et al., 2020; Arikibe et al., 2021; Kalyani & Khandelwal, 2021). The appearance of N-H bending and C=O stretching amide absorption indicates that the Chi used has a degree of deacetylation below 100%. Typical TiO_2 and ZnO absorption appeared in the fingerprint region at wave numbers 648 and 559-674 cm^{-1} respectively (Rahmi et al., 2021; Shafiq et al., 2013).

The O-H absorption peak in the composite, which includes Gr, TiO_2, and ZnO, has moved to a lower wavenumber than the O-H peak in Chi/BC (3274 cm^{-1}). This indicates an interaction between the filler, Chi, and BC. The addition of TiO_2 and ZnO results in the widening of the O-H peak due to the formation of hydrogen bonds. This is discussed by Anaya-Esparza et al. (2020) and Ekanayake & Godakumbura (2021). Figure 8 illustrates the hydrogen bonding of Chi and BC with TiO_2 and ZnO.
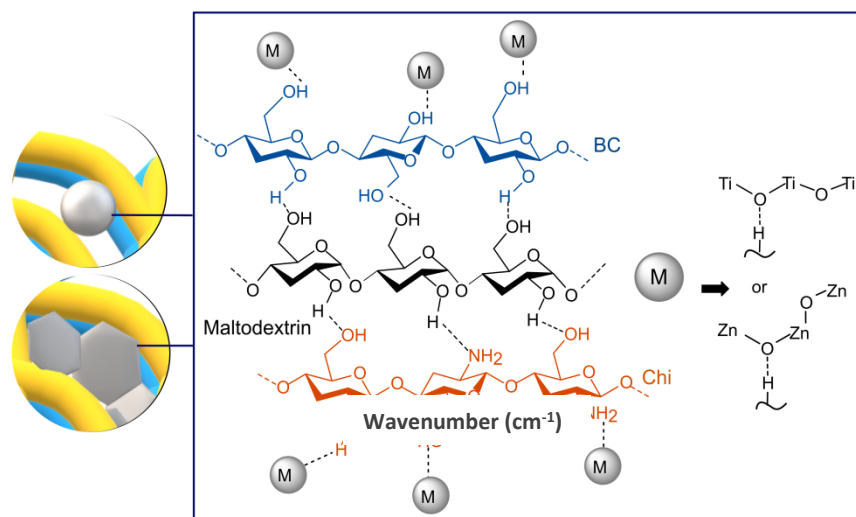

Figure 8. Hydrogen Bonds Between Chi and BC with TiO_2 and ZnO

According to Palanisamy et al. (2016), adding Gr to Chi decreases the intensity of N-H, C=O, and CH_2 bending absorption. This is believed to be caused by interfacial adhesion between Gr and Chi. The interaction between the two materials is illustrated in Figure 9, which shows that the amine groups in the acidic solution can interact with the π bonds of Gr, producing cation-π interactions. As a result of this interaction, the absorption peak of C-H bending disappears.

Adding TiO_2 and ZnO increases the intensity of N-H, C=O, and CH_2 bending. Chi and TiO_2 interact through hydrogen bonding and electrostatic forces between the $-NH_2$ group and Ti atoms. Similarly, Chi and ZnO also interact through hydrogen bonding, as ZnO particles bond with $-NH_2$ groups. Unagglomerated ZnO particles create Zn^{2+} ions that form electrostatic interactions with Chi (Ekanayake & Godakumbura, 2021). Figure 10 illustrates the electrostatic interaction between ZnO and TiO_2 particles with Chi. The figure suggests that free electrons in the amine group create an attractive force towards Ti atoms and Zn ions.
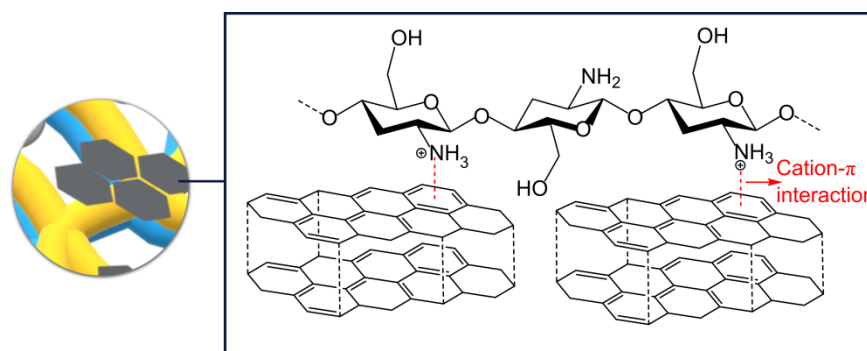

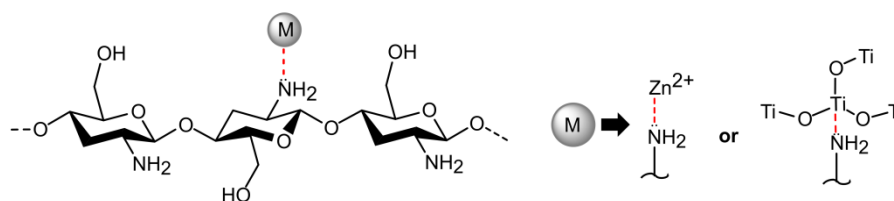**Figure 9.** Interaction Between Chi and Gr

Figure 10. Electrostatic Interaction of Chi with TiO$_2$ and ZnO

Antibacterial Activity

The effectiveness of the antibacterial properties of the composite material is demonstrated in Figure 11. The graph in Figure 12 depicts the level of inhibition zone of the composite against bacteria. A filter paper soaked in TCH solution was used as the positive control for the experiment.

The tested composite material did not show any antibacterial activity against *S. aureus*. This was because the composite did not contain TCH. However, the composite containing Gr, TiO$_2$, and ZnO is expected to be antibacterial. The absence of an inhibition zone on the composite material could be attributed to using maltodextrin as a cross-linking agent. Previous studies have shown that maltodextrin can reduce the inhibitory

ability of active substances against bacteria (Hasanuddin et al., 2019). This is because maltodextrin can block the film's diffusion pathway and reduce antibacterial agents' effectiveness (Kiamco et al., 2015).

The composite material that includes TCH has been found to have a higher bacterial inhibition rate than the positive control (filter paper soaked with TCH). This suggests that the composite material could be used as a drug carrier agent. Chi/BC/Gr/ZnO is one of the composites tested and showed the highest inhibition zone. This was mainly due to the TCH loading process, where pre-soaking the composite material in an acidic TCH solution allowed more TCH molecules to enter the pores of Chi/BC/Gr/ZnO, which has optimal swelling properties in acidic pH. As the percentage of swelling increases, the amount of drug contained in the composite material also increases (Mali et al., 2018).
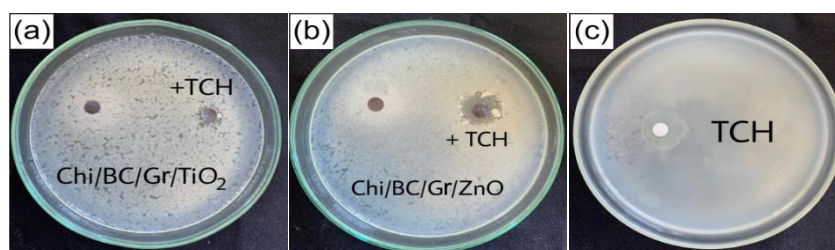

Figure 11. Antibacterial Activity of (a) Chi/BC/Gr/TiO$_2$, (b) Chi/BC/Gr/ZnO, and (c) Positive Control
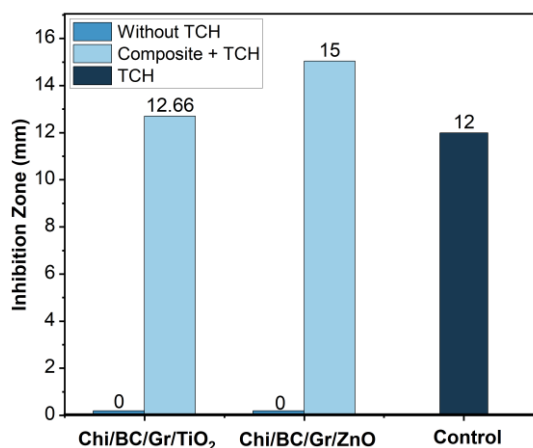

Figure 12. Inhibition Zone of Composites

Drug Release Kinetics

The graphs in Figure 13 illustrate the results of the kinetics test data plots. Table 4 presents the R^2 and k values for each kinetics model. The release of TCH from the matrix in this experiment happened in two stages. The Chi/BC/Gr/TiO$_2$ composite followed the Hixson-Crowell kinetics model in both stages, with the R^2 value being 0.9971 in the

first stage and 0.8666 in the second stage. Due to surface erosion, the composite tends to release TCH parallel to the composite plane (Tian et al., 2020). The process of TCH release is affected by the surface area of the composite (Bruschi, 2015). The composite size can be adjusted to control the drug release system with this composite based on the factors that affect the drug release mechanism of the Chi/BC/Gr/TiO$_2$ composite (Abukhadra et al., 2019).

Table 4. R^2 and k Values of Composites Based on Several Kinetics Models.

| Composite	Zero Order		First Order		Higuchi		Hixson-Crowell		Korsmeyer-Peppas	
	R^2	k	R^2	k	R^2	k	R^2	k	R^2	K
Chi/BC/Gr/TiO$_2$*	0.9961	0.1	0.9955	0.0009	0.9928	1.9	0.9971	0.003	0.9765	0.1
Chi/BC/Gr/ZnO*	0.8947	0.2	0.8880	0.0019	0.9366	3.6	0.8976	0.005	0.9631	0.3
Chi/BC/Gr/TiO$_2$**	0.8505	0.1	0.8362	0.0006	0.8282	2.6	0.8666	0.003	0.8001	0.3
Chi/BC/Gr/ZnO**	0.8608	0.1	0.8554	0.0009	0.8430	3.7	0.8655	0.004	0.8186	0.4

*First stage   **Second stage
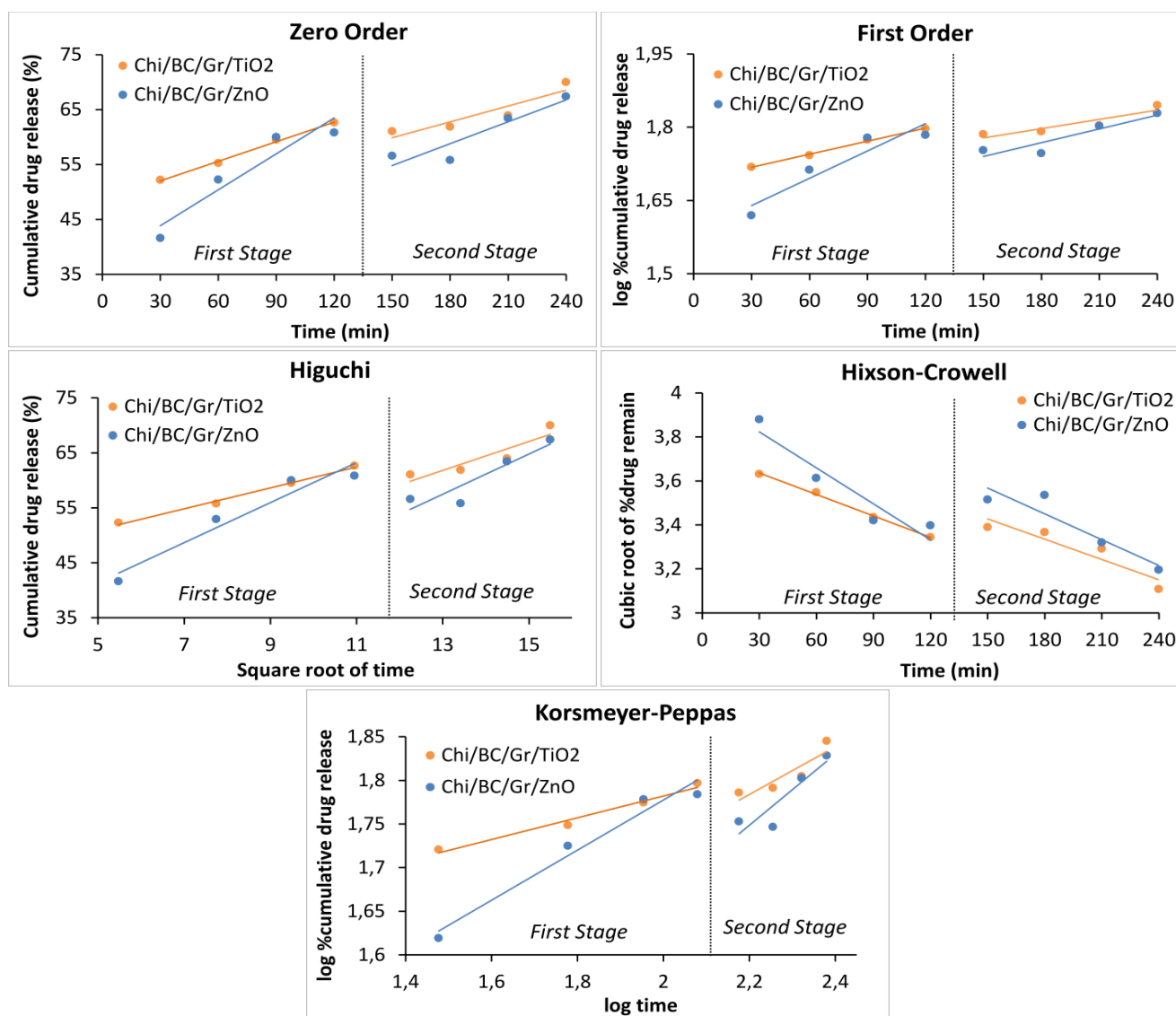
Figure 13. Plotting Results of Several Kinetics Models

The Chi/BC/Gr/ZnO composite drug release was analyzed using the Korsmeyer-Peppas kinetics model. The R^2 value obtained was 0.9631, indicating that the drug release in the first stage followed this model. The diffusion exponent (n) value is 0.3, less than 0.5. Therefore, the drug release mechanism from the composite is considered to follow the pseudo-Fickian diffusion mechanism, according to Bayer's study in 2023. This mechanism is like the Fickian model, except that the final equilibrium of solvent absorption by the composite is slower in the pseudo-Fickian model, resulting in a slower drug diffusion process, as found in Bercea et al.'s study in 2016. This suggests that the drug release from Chi/BC/Gr/ZnO composites between 30 to 120 minutes is mainly controlled by the drug diffusion process rather than the swelling or relaxation process of the matrix polymer chains, as stated in Bruschi's study in 2015. In the second stage, drug release followed the Hixson-Crowell kinetics model, indicating that from the 150th to the 240th minute, drug release tends to be influenced by erosion.

Conclusion

Composites of Chi/BC/Gr/TiO$_2$ and Chi/BC/Gr/ZnO were successfully created and used as drug carrier systems. The release of TCH from the Chi/BC/Gr/ TiO$_2$ composite followed the Hixson-Crowell kinetics model in both stages. In contrast, the Chi/BC/Gr/ZnO release followed the Korsmeyer-Peppas kinetics model in the first stage and Hixson-Crowell in the second stage. Incorporating Gr, TiO$_2$, and ZnO fillers improved the physical and mechanical properties of the composites compared to the Chi/BC composites. Additionally, composites that contained TCH showed higher antibacterial activity than the positive control.

Conflict of Interest

The authors declare that there is no conflict of interest.

Acknowledgments

References

Abukhadra, M. R., Refay, N. M., El-Sherbeeny, A. M., Mostafa, A. M., & Elmeligy, M. A. (2019). Facile synthesis of bentonite/biopolymer composites as low-cost carriers for 5-fluorouracil drug; equilibrium studies and pharmacokinetic behavior. *International Journal of Biological Macromolecules*, 141. https://doi.org/10.1016/j.ijbiomac.2019.09.057

Adepu, S., & Ramakrishna, S. (2021). Controlled drug delivery systems: Current status and future directions. *Molecules*, 26(19). https://doi.org/10.3390/molecules26195905

Anaya-Esparza, L. M., Ruvalcaba-Gómez, J. M., Maytorena-Verdugo, C. I., González-Silva, N., Romero-Toledo, R., Aguilera-Aguirre, S., Pérez-Larios, A., & Montalvo-González, E. (2020). Chitosan-tio2: A versatile hybrid composite. *Materials*, 13(4). https://doi.org/10.3390/ma13040811

Arikibe, J. E., Lata, R., & Rohindra, D. (2021). Bacterial Cellulose/Chitosan Hydrogels Synthesized In situ for Biomedical Application. *Journal of Applied Biosciences*, 162, 16675–16693. https://doi.org/10.35759/jabs.162.1

Bayer, I. S. (2023). Controlled Drug Release from Nanoengineered Polysaccharides. In *Pharmaceutics* (Vol. 15, Issue 5). https://doi.org/10.3390/pharmaceutics15051364

Bercea, M., Morariu, S., & Teodorescu, M. (2016). Rheological investigation of poly(vinyl alcohol)/poly(N-vinyl pyrrolidone) mixtures in aqueous solution and hydrogel state. *Journal of Polymer Research*, 23(7). https://doi.org/10.1007/s10965-016-1040-3

Bruschi, M. L. (2015). Strategies to Modify the Drug Release from Pharmaceutical Systems. In M. L. Bruschi (Ed.), *Strategies to Modify the Drug Release from Pharmaceutical Systems*. Elsevier.

Cai, L., Wang, Y., & Cao, A. (2020). The physiochemical and preservation properties of fish sarcoplasmic protein/chitosan composite films containing ginger essential oil emulsions. *Journal of Food Process Engineering*, 43(10), 1–12. https://doi.org/10.1111/jfpe.13495

Chahardahmasoumi, S., Sarvi, M. N., & Jalali, S. A. H. (2019). Modified montmorillonite nanosheets as a nanocarrier with smart pH-responsive control on the antimicrobial activity of tetracycline upon release. *Applied Clay Science*, 178. https://doi.org/10.1016/j.clay.2019.105135

Choi, S. M., & Shin, E. J. (2020). The nanofication and functionalization of bacterial cellulose and its applications. In *Nanomaterials* (Vol. 10, Issue 3). https://doi.org/10.3390/nano10030406

Ekanayake, S. A., & Godakumbura, P. I. (2021). Synthesis of a Dual-Functional Nanofertilizer by Embedding ZnO and CuO Nanoparticles on an Alginate-Based Hydrogel. *ACS Omega*, 6(40). https://doi.org/10.1021/acsomega.1c03271

El-Alfy, E. A., El-Bisi, M. K., Taha, G. M., & Ibrahim, H. M. (2020). Preparation of biocompatible chitosan nanoparticles loaded by tetracycline, gentamycin, and ciprofloxacin as novel drug delivery system for improvement the antibacterial properties of cellulose

based fabrics. *International Journal of Biological Macromolecules*, 161. https://doi.org/10.1016/j.ijbiomac.2020.06.118

Fakhri, E., Eslami, H., Maroufi, P., Pakdel, F., Taghizadeh, S., Ganbarov, K., Yousefi, M., Tanomand, A., Yousefi, B., Mahmoudi, S., & Kafil, H. S. (2020). Chitosan biomaterials application in dentistry. In *International Journal of Biological Macromolecules* (Vol. 162). https://doi.org/10.1016/j.ijbiomac.2020.06.211

Fan, X., Chen, K., He, X., Li, N., Huang, J., Tang, K., Li, Y., & Wang, F. (2016). Nano-TiO2/collagen-chitosan porous scaffold for wound repairing. *International Journal of Biological Macromolecules*, 91, 15–22. https://doi.org/10.1016/j.ijbiomac.2016.05.094

Farzamfar, S., Naseri-Nosar, M., Sahrapeyma, H., Ehterami, A., Goodarzi, A., Rahmati, M., Ahmadi Lakalayeh, G., Ghorbani, S., Vaez, A., & Salehi, M. (2019). Tetracycline hydrochloride-containing poly (ε-caprolactone)/poly lactic acid scaffold for bone tissue engineering application: in vitro and in vivo study. *International Journal of Polymeric Materials and Polymeric Biomaterials*, 68(8), 472–479. https://doi.org/10.1080/00914037.2018.1466133

Fasiku, V. O., Omolo, C. A., Devnarain, N., Ibrahim, U. H., Rambharose, S., Faya, M., Mocktar, C., Singh, S. D., & Govender, T. (2021). Chitosan-Based Hydrogel for the Dual Delivery of Antimicrobial Agents against Bacterial Methicillin-Resistant Staphylococcus aureus Biofilm-Infected Wounds. *ACS Omega*, 6(34). https://doi.org/10.1021/acsomega.1c02547

Flores, F. P., & Kong, F. (2017). In Vitro Release Kinetics of Microencapsulated Materials and the Effect of the Food Matrix. *Annual Review of Food Science and Technology*, 8(January), 237–259. https://doi.org/10.1146/annurev-food-030216-025720

George, D., Maheswari, P. U., Sheriffa Begum, K. M. M., & Arthanareeswaran, G. (2019). Biomass-Derived Dialdehyde Cellulose Cross-linked Chitosan-Based Nanocomposite Hydrogel with Phytosynthesized Zinc Oxide Nanoparticles for Enhanced Curcumin Delivery and Bioactivity. *Journal of Agricultural and Food Chemistry*, 67(39). https://doi.org/10.1021/acs.jafc.9b01933

Hasanuddin, A., Anwar, K., Mappatoba, M., & Hafsah. (2019). Antibacterial and Antioxidant Activities of Ethanol Extracts of Cocoa Husk (Theobroma cacao L.) with Maltodextrine in Various Concentration. *IOP Conference Series: Earth and Environmental Science*, 255(1). https://doi.org/10.1088/1755-1315/255/1/012017

Hosseini, S. M., Mazinani, S., Abdouss, M., Kalhor, H., Kalantari, K., Amiri, I. S., & Ramezani, Z. (2022). Designing chitosan nanoparticles embedded into graphene oxide as a drug delivery system. *Polymer Bulletin*, 79(1). https://doi.org/10.1007/s00289-020-03506-8

Hussein, E. M., Desoky, W. M., Hanafy, M. F., & Guirguis, O. W. (2021). Effect of TiO2 nanoparticles on the structural configurations and thermal, mechanical,

and optical properties of chitosan/TiO2 nanoparticle composites. *Journal of Physics and Chemistry of Solids*, 152. https://doi.org/10.1016/j.jpcs.2021.109983

Iftime, M. M., Dobreci, D. L., Irimiciuc, S. A., Agop, M., Petrescu, T., & Doroftei, B. (2020). A theoretical mathematical model for assessing diclofenac release from chitosan-based formulations. *Drug Delivery*, 27(1), 1125–1133. https://doi.org/10.1080/10717544.2020.1797242

Kalemtas, A., Kocer, H. B., Aydin, A., Terzioglu, P., & Aydin, G. (2022). Mechanical and antibacterial properties of ZnO/chitosan bio-composite films. *Journal of Polymer Engineering*, 42(1). https://doi.org/10.1515/polyeng-2021-0143

Kalyani, P., & Khandelwal, M. (2021). Modulation of morphology, water uptake/retention, and rheological properties by in-situ modification of bacterial cellulose with the addition of biopolymers. *Cellulose*, 28(17), 11025–11036. https://doi.org/10.1007/s10570-021-04256-0

Kamaludin, R., Majid, L. A., Othman, M. H. D., Mansur, S., Sheikh Abdul Kadir, S. H., Wong, K. Y., Khongnakorn, W., & Puteh, M. H. (2022). Polyvinylidene Difluoride (PVDF) Hollow Fiber Membrane Incorporated with Antibacterial and Anti-Fouling by Zinc Oxide for Water and Wastewater Treatment. *Membranes*, 12(2). https://doi.org/10.3390/membranes12020110

Kiamco, M. M., Atci, E., Khan, Q. F., Mohamed, A., Renslow, R. S., Abu-Lail, N., Fransson, B. A., Call, D. R., & Beyenal, H. (2015). Vancomycin and maltodextrin affect structure and activity of Staphylococcus aureus biofilms. *Biotechnology and Bioengineering*, 112(12). https://doi.org/10.1002/bit.25681

Laksmono, J. A., Sudibandriyo, M., Saputra, A. H., & Haryono, A. (2017). Development of porous structured polyvinyl alcohol/zeolite/carbon composites as adsorbent. *IOP Conference Series: Materials Science and Engineering*, 201(1). https://doi.org/10.1088/1757-899X/201/1/012006

Laracuente, M. L., Yu, M. H., & McHugh, K. J. (2020). Zero-order drug delivery: State of the art and future prospects. In *Journal of Controlled Release* (Vol. 327). https://doi.org/10.1016/j.jconrel.2020.09.020

Li, Y., Chi, Y. Q., Yu, C. H., Xie, Y., Xia, M. Y., Zhang, C. L., Han, X., & Peng, Q. (2020). Drug-free and non-crosslinked chitosan scaffolds with efficient antibacterial activity against both Gram-negative and Gram-positive bacteria. *Carbohydrate Polymers*, 241. https://doi.org/10.1016/j.carbpol.2020.116386

Lu, Y., Liang, L., Shen, G., Yao, W., Zhang, C., Huang, D., Xuan, Z., Li, J., & Liu, J. (2022). Theoretical Investigation of Chitosan-Assisted Controlled Release of Digestive System Antitumor Drug Fluorouracil. *Journal of Pharmaceutical Sciences*, 111(7). https://doi.org/10.1016/j.xphs.2022.01.034

Mali, K. K., Dhawale, S. C., Dias, R. J., Dhane, N. S., & Ghorpade, V. S. (2018). Citric acid crosslinked carboxymethyl cellulose-based composite hydrogel

films for drug delivery. *Indian Journal of Pharmaceutical Sciences*, 80(4). https://doi.org/10.4172/pharmaceutical-sciences.1000405

Mirzaeei, S., Moghadam, F., Asare-Addo, K., & Nokhodchi, A. (2022). Design of a nanofibrous guided tissue regeneration carrier as a potential drug delivery system for tetracycline hydrochloride in the management of periodontitis. *Journal of Drug Delivery Science and Technology*, 75. https://doi.org/10.1016/j.jddst.2022.103722

Orylska-Ratynska, M., Placek, W., & Owczarczyk-Saczonek, A. (2022). Tetracyclines—An Important Therapeutic Tool for Dermatologists. In *International Journal of Environmental Research and Public Health* (Vol. 19, Issue 12). https://doi.org/10.3390/ijerph19127246

Palanisamy, S., Thangavelu, K., Chen, S. M., Gnanaprakasam, P., Velusamy, V., & Liu, X. H. (2016). Preparation of chitosan grafted graphite composite for sensitive detection of dopamine in biological samples. *Carbohydrate Polymers*, 151, 401–407. https://doi.org/10.1016/j.carbpol.2016.05.076

Pomari, A. A. D. N., Montanheiro, T. L. D. A., de Siqueira, C. P., Silva, R. S., Tada, D. B., & Lemes, A. P. (2019). Chitosan hydrogels crosslinked by genipin and reinforced with cellulose nanocrystals: Production and characterization. *Journal of Composites Science*, 3(3). https://doi.org/10.3390/jcs3030084

Rahimi, M., Charmi, G., Matyjaszewski, K., Banquy, X., & Pietrasik, J. (2021). Recent developments in natural and synthetic polymeric drug delivery systems used for the treatment of osteoarthritis. In *Acta Biomaterialia* (Vol. 123). https://doi.org/10.1016/j.actbio.2021.01.003

Rahmi, Lubis, S., & Az-Zahra, N. (2021). Effect of Cellulose and Titanium Dioxide on the properties of Chitosan film. *Journal of Physics: Conference Series*, 1882(1). https://doi.org/10.1088/1742-6596/1882/1/012105

Rais, A., Sembiring, T., Humaidi, S., & Hakim, A. (2022). The effect of ZnO - TiO2 synthesis analysis using sol-gel method on calcination temperature of thin film as an alternative energy materials. *Journal of Physics: Conference Series*, 2193(1). https://doi.org/10.1088/1742-6596/2193/1/012047

Shafiq, M., Yasin, T., Rafiq, M. A., & Shaista. (2013). Structural, Thermal, and Antibacterial Properties of Chitosan/ZnO. *Polymers and Polymer Composites*, 35, 22636–22643. https://doi.org/10.1002/pc

Sun, X., Yin, L., Zhu, H., Zhu, J., Hu, J., Luo, X., Huang, H., & Fu, Y. (2022). Enhanced Antimicrobial Cellulose/Chitosan/ZnO Biodegradable Composite Membrane. *Membranes*, 12(2). https://doi.org/10.3390/membranes12020239

Suryanegara, L., Fatriasari, W., Zulfiana, D., Anita, S. H., Masruchin, N., Gutari, S., & Kemala, T. (2021). Novel antimicrobial bioplastic based on PLA-chitosan by addition of TiO2 and ZnO. *Journal of Environmental Health Science and Engineering*, 19(1). https://doi.org/10.1007/s40201-021-00614-z

Tavakoli, M., Karbasi, S., & Soleymani Eil Bakhtiari, S. (2020). Evaluation of physical, mechanical, and biodegradation of chitosan/graphene oxide composite as bone substitutes. *Polymer-Plastics Technology and Materials*, 59(4). https://doi.org/10.1080/25740881.2019.1653467

Tian, L., Abukhadra, M. R., Mohamed, A. S., Nadeem, A., Ahmad, S. F., & Ibrahim, K. E. (2020). Insight into the Loading and Release Properties of an Exfoliated Kaolinite/Cellulose Fiber (EXK/CF) Composite as a Carrier for Oxaliplatin Drug: Cytotoxicity and Release Kinetics. *ACS Omega*, 5(30), 19165–19173. https://doi.org/10.1021/acsomega.0c02529

Turan, B., Sarigol, G., & Demircivi, P. (2022). Adsorption of tetracycline antibiotics using metal and clay embedded cross-linked chitosan. *Materials Chemistry and Physics*, 279. https://doi.org/10.1016/j.matchemphys.2022.125781

Ulfa, M., Noviani, I., Yuanita, E., Dharmayani, N. K. T., Sudirman, & Sarkono. (2023). Synthesis and Characterization of Composites-Based Bacterial Cellulose by Ex-Situ Method as Separator Battery. *Jurnal Penelitian Pendidikan IPA*, 9(6). https://doi.org/10.29303/jppipa.v9i6.3819

Wahba, M. I. (2020). Enhancement of the mechanical properties of chitosan. *Journal of Biomaterials Science, Polymer Edition*, 31(3), 350–375. https://doi.org/10.1080/09205063.2019.1692641

Wahid, F., Hu, X. H., Chu, L. Q., Jia, S. R., Xie, Y. Y., & Zhong, C. (2019). Development of bacterial cellulose/chitosan based semi-interpenetrating hydrogels with improved mechanical and antibacterial properties. *International Journal of Biological Macromolecules*, 122, 380–387. https://doi.org/10.1016/j.ijbiomac.2018.10.105

Xu, H., Li, D., Liu, Y., Jiang, Y., Li, F., & Xue, B. (2019). Preparation of halloysite/polyvinylidene fluoride composite membrane by phase inversion method for lithium ion battery. *Journal of Alloys and Compounds*, 790, 305–315. https://doi.org/10.1016/j.jallcom.2019.03.075

Yasmeen, S., Kabiraz, M., Saha, B., Qadir, M., Gafur, M., & Masum, S. (2016). Chromium (VI) Ions Removal from Tannery Effluent using Chitosan-Microcrystalline Cellulose Composite as Adsorbent. *International Research Journal of Pure and Applied Chemistry*, 10(4), 1–14. https://doi.org/10.9734/irjpac/2016/23315

Yenier, Z., Seki, Y., Şen, I., Sever, K., Mermer, Ö., & Sarikanat, M. (2016). Manufacturing and mechanical, thermal and electrical characterization of graphene loaded chitosan composites. *Composites Part B: Engineering*, 98, 281–287. https://doi.org/10.1016/j.compositesb.2016.04.072